Frontiers of Information Technology & Electronic Engineering
www.jzus.zju.edu.cn; engineering.cae.cn; www.springerlink.com
ISSN 2095-9184 (print); ISSN 2095-9230 (online)
E-mail: jzus@zju.edu.cn

Review:

Super-resolution optical microscope: principle, instrumentation, and application*

Bao-kai WANG[1], Martina BARBIERO[1], Qi-ming ZHANG[1], Min GU[†‡1,2]

[1]*Laboratory of Artificial-Intelligence Nanophotonics, School of Science, RMIT University, Melbourne, Victoria 3001, Australia*

[2]*Center for Artificial-Intelligence Nanophotonics, School of Optical-Electrical and Computer Engineering, University of Shanghai for Science and Technology, Shanghai 200093, China*

[†]E-mail: gumin@usst.edu.cn

Received July 27, 2018; Revision accepted Oct. 29, 2018; Crosschecked May 13, 2019

Abstract: Over the past two decades, several fluorescence- and non-fluorescence-based optical microscopes have been developed to break the diffraction limited barrier. In this review, the basic principles implemented in microscopy for super-resolution are described. Furthermore, achievements and instrumentation for super-resolution are presented. In addition to imaging, other applications that use super-resolution optical microscopes are discussed.

Key words: Super-resolution; Imaging; Optical microscope
https://doi.org/10.1631/FITEE.1800449 **CLC number:** O439

1 Introduction

The maximum spatial resolution of a conventional optical microscope is limited to half the wavelength of light. The limitation is due to the diffraction barrier imposed by the slight bending of a light beam when it encounters an object. According to Abbe (1873), a light beam of wavelength λ focused by a lens with numerical aperture $n\sin\alpha$ ($\sin\alpha<1$) cannot resolve objects closer than distance $d=\lambda/(2n\sin\alpha)$ (Gu, 1996, 2000). The diffraction of light causes a sharp pointed object to blur into a finite-sized image spot through the optical microscope.

The resolution of microscopes is determined by the size of the point spread function (PSF). The PSF is defined as the three-dimensional (3D) intensity distribution of the image of a point object. Another approach for determining the resolution of a microscope in the frequency domain is by measuring the cut-off frequency of the optical transfer function (OTF). OTF is the Fourier transform of PSF (Gu, 2000).

In the visible wavelength region, the resolution of a conventional optical microscope is around 200–300 nm in the lateral direction and 500–700 nm in the axial direction.

In 2014, the Nobel Prize in Chemistry was awarded jointly to Eric BETZIG, Stefan W. HELL, and William E. MOERNER for the development of super-resolution fluorescence microscopes that allow the imaging resolution limitation due to the diffraction of light to be overcome. Stefan W. HELL was the first scientist to break the diffraction barrier theoretically (Hell and Wichmann, 1994) and experimentally (Klar and Hell, 1999) with the concept of stimulated emission depletion (STED). Eric BETZIG (Betzig, 1995; Betzig et al., 2006) pioneered the method called photoactivated localization microscopy (PALM) in 2006. William E. MOERNER's contributions center on the first optical detection and spectroscopy of a single molecule in condensed phases (Moerner and

‡ Corresponding author
* Project supported by the Australian Research Council (ARC) through the Discovery Project (No. DP170101775)
ORCID: Min GU, http://orcid.org/0000-0003-4078-253X

Kador, 1989) and on the observations of on/off blinking and switching behavior of green fluorescent protein (GFP) mutants at room temperature (Dickson et al., 1997).

In recent years, a number of novel super-resolution fluorescence- and non-fluorescence-based methods have been developed. The fluorescence-based methods are further divided into spatial- and time-domain techniques.

In this review, we summarize the basic principles implemented in fluorescence- and non-fluorescence-based optical microscopy. We also review the achievements and developments of these optical microscopes, as well as their applications to other fields.

2 Principle

2.1 Fluorescence-based super-resolution

2.1.1 Spatial-domain methods

1. Saturated structured-illumination microscopy

Structured-illumination microscopy (SIM) achieves spatial resolution beyond the diffraction limit with a wide-field microscope with spatially structured illumination.

A grating is used to generate a structured illumination pattern that varies in lateral direction (Gustafsson, 2000) (Fig. 1a) or three dimensions (Gustafsson et al., 2008). The structured illumination extends resolution beyond the cut-off by moving high-frequency information into the observed images in the form of Moiré fringes. The Moiré fringes are generated through spatial frequency mixing (Fig. 1c). The new image is computationally extracted. The method demonstrates imaging with twice the spatial resolution of conventional microscopes.

SIM is applied in three dimensions to double the axial and lateral resolutions. Resolutions of about 100 nm in the lateral direction and about 300 nm in the axial direction were obtained (Schermelleh et al., 2008; Shao et al., 2011).

In saturated structured-illumination microscopy (SSIM), a nonlinear phenomenon, the saturation of fluorescence emission, is applied to achieve a theoretical unlimited resolution (Gustafsson, 2005). The saturation occurs when a fluorophore is illuminated by optical intensities in the order of about 10^6 W/cm^2.

Under an excitation beam with high optical intensity, a fluorophore in the ground state is immediately pumped to the excited state. The fluorescence lifetime is determined by the fluorescent emission rate. When the fluorophore reaches saturation, its fluorescence is not proportional to the intensity of the excitation light. Under this circumstance, a saturated excitation structured illumination pattern is achieved. When the intensity reaches the saturated level, the pattern becomes flat (Fig. 1b).

Higher frequency information is encoded by mixing saturated excitation structured illumination patterns containing more Fourier components (Fig. 1c).

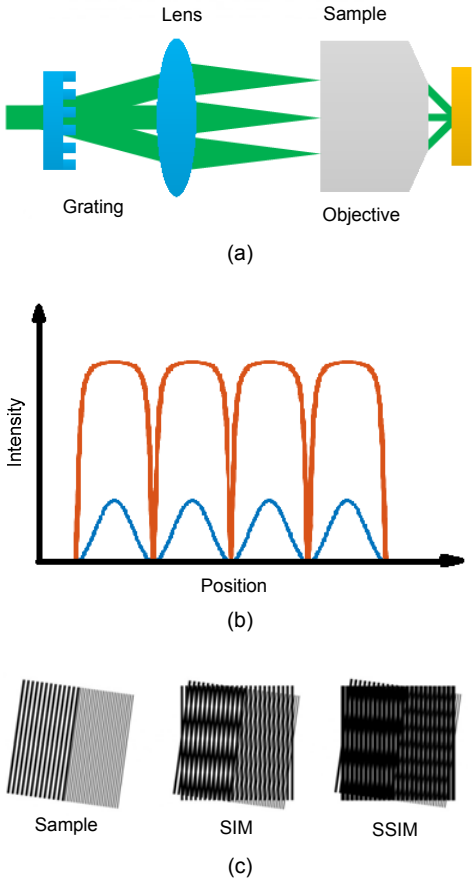

Fig. 1 Principles of structured-illumination microscopy (SIM) and saturated structured-illumination microscopy (SSIM): (a) structured illumination generated by a grating; (b) SIM excitation pattern (blue line) and SSIM excitation pattern (red line); (c) imaging the sample with SIM and SSIM

References to color refer to the online version of this figure

The resolving power is determined by the signal-to-noise ratio, which in turn is limited by photobleaching. Experimental results showed that a

two-dimensional (2D) point resolution of less than 50 nm was possible to achieve with bright photostable samples (Gustafsson, 2005) and photoswitchable proteins (Rego et al., 2012; Li et al., 2015).

2. Image scanning microscopy

Image scanning microscopy (ISM) was previously described by Sheppard (1988) and demonstrated by Müller and Enderlein (2010). ISM doubles the resolution of a scanning confocal image. The principle of ISM is to extract the inherent high-frequency information from a laser scanning confocal microscope (LSCM). The origin of the super-resolution information can be understood in two different ways. The first way is to describe the origin based on the idea of overlapping excitation and emission PSFs in an LSCM (Sheppard, 1988; Sheppard et al., 2013); the second description is the same as SIM (Müller and Enderlein, 2010). The super-resolution information can be collected simply by reducing the size of the pinhole in an LSCM. However, a smaller pinhole rejects a large amount of light, reducing the signal-to-noise ratio. ISM can recover the lost super-resolution information. The optical setup of ISM involves recording the signal that passes through the pinhole on an array detector and obtaining an image at each scanning position. The simplest way to recover a final super-resolution image is pixel reassignment (Sheppard et al., 2013). For every scanning position, the image obtained is reduced by some factor, and added to a running-total image that is centered at the scanning position of the beam. After a complete picture has been reconstructed, further resolution enhancement can be achieved by Fourier reweighting.

To achieve faster acquisition, a digital micromirror device (DMD) is applied to obtain multifocal structured illumination in ISM (York et al., 2012). Following this idea, ISM is also achieved in a confocal spinning-disk microscope (Schulz et al., 2013), but these approaches still require recording and storing vast amounts of data for reconstructing a super-resolved image and reducing acquisition speed. This problem is solved by all-optical ISM based on rescanning (de Luca et al., 2013; Roth et al., 2013; York et al., 2013; Azuma and Kei, 2015). All-optical ISM based on rescanning is also applied for two-photon-excited fluorescence and second-harmonic generation imaging (Gregor et al., 2017).

3. Stimulated emission depletion

The concept of STED microscopy was first proposed by Hell and Wichmann (1994), and demonstrated experimentally in Klar and Hell (1999). Super-resolution is achieved through the selective deactivation of fluorophores via stimulated emission. Under a depletion beam, a fluorophore in the excited state interacts with a photon that matches the energy difference between the excited state and the ground state (Fig. 2a). In this case, the fluorescence emission of the fluorophore is depleted.

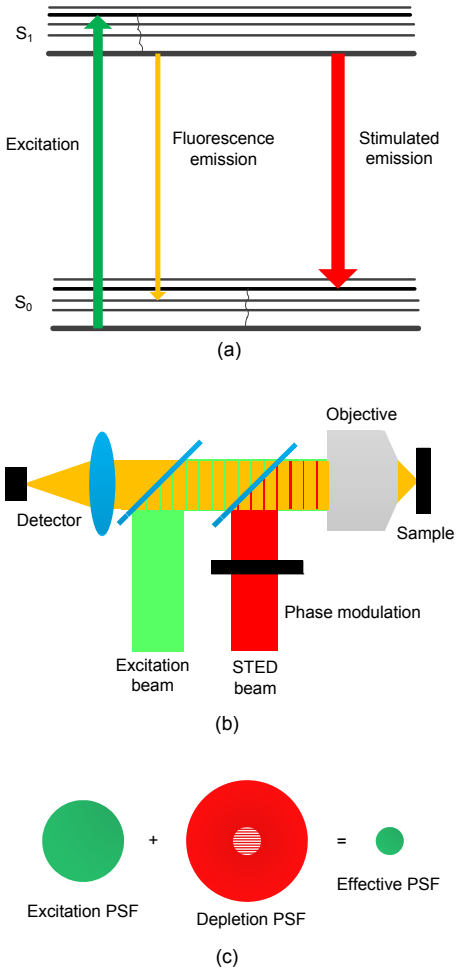

Fig. 2 Principle of the stimulated emission depletion (STED) microscope: (a) Jablonski diagram of the process of fluorescence emission and stimulated emission; (b) schematic of an STED microscope; (c) effective point spread function (PSF) generated

The optical setup of STED is based on a confocal microscope. The excitation beam and STED beam are

scanned across the sample (Fig. 2b). The STED beam is generated by a continuous-wave (CW) or a pulsed-laser source. A phase mask is inserted in the path of the STED light to create a doughnut-shaped beam with zero fields at the center and non-zero fileds at the periphery. Therefore, the effective excitation PSF becomes sharper (Fig. 2c).

In pulsed-mode STED, the time delay between the excitation and STED laser beams is of paramount importance in optimizing the stimulated emission. The STED beam reaches the sample when the electron is in the excited state. Furthermore, the pulse width of the STED laser beam is tuned to a value between the lifetimes of the vibrational states and the excited state of a dye, e.g., 200–300 ps.

In CW STED (Willig et al., 2007), CW excitation at a rate k_{exc} populates the excited state with probability $N=k_{exc}/(k_{exc}+k_{fl})$; fluorescent decay rate $k_{fl}=1/\tau_{fl}$ is given by the inverse of the lifetime of the excited state. The addtion of a CW STED beam provides another decay rate $k_{STED}=\sigma I$, yielding $N=k_{exc}/(k_{exc}+k_{fl}+k_{STED})$, where σ is the molecular cross-section for stimulated emission and I the intensity of the STED beam in photons per area and per second. STED becomes predominant when $k_{STED}>k_{exc}>k_{fl}$, which means $I>1/(\sigma\tau_{fl})$. The power of the CW beam is about 3.6 times larger than the time-averaged power of the pulsed mode. However, CW STED greatly simplifies the implementation of STED superresolution microscopy by removing the synchronization units needed in pulsed systems.

The wavelength of the depletion photon should also be in the range of the emission wavelength of the dye. Therefore, the wavelength of the STED beam is selected to be at the end of the emission spectrum of the dye, avoiding re-absorption. The higher the cross sections of the STED beam and emission spectrum are, the higher the stimulated absorption cross section is. Therefore, a higher resolution is obtained (Farahani et al., 2010).

There are two factors that determine the resolution of STED microscopy: the STED laser beam intensity and the saturation intensity of the fluorophore. The latter is a function of the STED laser beam wavelength, pulse width, and intrinsic characteristics of the fluorophore such as lifetime and kinetics of the population of ground and excited states. This is mathematically described in the extended version of the optical resolution limit defined by Westphal and Hell (2005):

$$d=\frac{\lambda}{2n\sin\alpha\sqrt{1+I/I_s}}, \tag{1}$$

where λ is the wavelength of the excitation beam, $n\sin\alpha$ determines the numerical aperture of the objective lens with n the refractive index of the medium and α half the focal angle, I is the intensity of the STED beam, and I_s is the saturation intensity of the fluorophore.

Normally, STED can achieve 20–60 nm lateral resolution (Westphal and Hell, 2005; Göttfert et al., 2013; Butkevich et al., 2016). STED can also be employed in 4Pi microscopy (STED-4Pi), resulting in an axial resolution of 30–40 nm (Dyba and Hell, 2002).

4. Ground-state-depletion microscopy

Ground state depletion (GSD) microscopy was proposed in Hell and Kroug (1995), and demonstrated experimentally in Bretschneider et al. (2007). The optical setup for GSD is based on confocal scanning microscopy. Typically, the fluorescent emitters can be freely excited from the ground state and return spontaneously. However, if a laser beam with an appropriate wavelength is applied, the dye is excited to a long-lived dark state (e.g., a triplet state). Therefore, the molecules in the long-lived dark state cannot be excited from the ground state (Bretschneider et al., 2007) (Fig. 3).

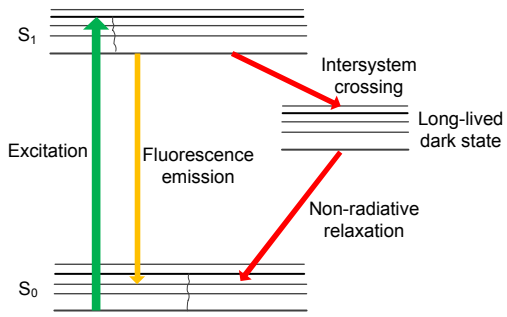

Fig. 3 Jablonski diagram of the process of fluorescence emission and long-lived dark state in a ground state depletion (GSD) microscope

Super-resolution imaging is achieved by applying a laser beam to deplete the ground state of the fluorophores within the doughnut area. The GSD

optical setup can be implemented with two different modalities. One needs two beams in the STED setup for depletion and excitation. The other one requires only one single doughnut shaped beam. Within the focal region except the doughnut minimum, the emitter is saturated in the excited state, and one "negative" image with sub-diffraction resolution is obtained upon scanning. The final image is achieved after the deconvolution of the "negative" image (Rittweger et al., 2009b).

Unlike STED, which features a high I_s value (about 10^7 W/cm^2) and thus requires an intense depletion laser beam (often >10^9 W/cm^2), GSD requires a low I_s (about 7 kW/cm^2). GSD enabled a resolution of 80 nm with a depletion laser beam intensity of 80 kW/cm^2 (Bretschneider et al., 2007).

5. Reversible saturable optically linear fluorescence transitions

Reversible saturable optically linear fluorescence transitions (RESOLFT) microscopy (Hell, 2007) has enabled achievement of super-resolution by suppressing undesired fluorescence emission through depletion. The optical setup for RESOLFT is based on a confocal scanning or a wide-field microscope. It is noted that the parallelized RESOLFT in a wide-field microscope uses orthogonally and incoherently crossed standing waves to generate a large number of doughnuts for parallelization (Chmyrov et al., 2013).

RESOLFT is applied on fluorescent probes that can be reversibly photoswitched between a fluorescent "on" state and a dark "off" state. The "on" state is the excited state. The "off" state can be the ground state of a fluorophore (Klar and Hell, 1999), or its triplet state (Bretschneider et al., 2007), or the dark state of a reversibly photoswitchable fluorophore (Hofmann et al., 2005) (Fig. 4).

The enhancement of the spatial resolution is obtained with a depletion laser beam to force the fluorophores at the periphery of the excitation into a dark state.

With I_{max} denoting the intensity bordering zero, the practical resolution is well approximated by

$$\Delta r \approx \frac{\lambda}{2n\sin\alpha\sqrt{1+I_{max}/I_s}}, \quad (2)$$

which differs from Abbe's equation because $I_{max}/I_s \to \infty$ implies an infinite resolution.

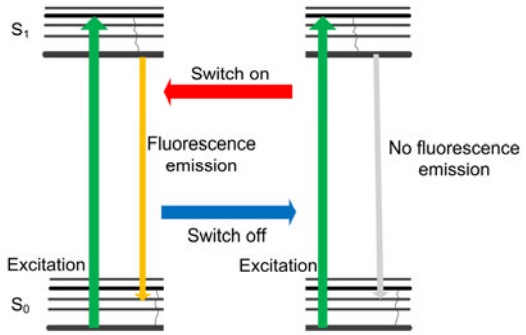

Fig. 4 Jablonski diagram of the process of fluorescence emission and long-lived dark state in a reversible saturable optically linear fluorescence transitions (RESOLFT) microscope with reversibly photoswitchable fluorophores

RESOLFT requires an optical transition that has a lower I_s. Therefore, super-resolution imaging is achieved with a much lower intensity for the depletion beam (Hell, 2007).

For example, RESOLFT has been demonstrated using a reversibly photoswitchable fluorescent protein (FP), as FP595, which led to a resolution better than 100 nm with a depletion laser beam intensity of 600 W/cm^2 (Hofmann et al., 2005). With the combination of 4Pi microscopy, an isotopic resolution below 40 nm was achieved when imaging an actin network inside the cells (Böhm et al., 2016).

RESOLFT nanoscopy with a low light intensity (60 W/cm^2) was also applied to image photoswitchable organic fluorophores with a spatial resolution of about 74 nm (Kwon et al., 2015).

2.1.2 Time-domain methods

1. Localization of single fluorophores

Single-molecule localization super-resolution microscopy enables reconstruction of the centroid position of spatially isolated fluorophores beyond the diffraction limit. An electron-multiplying charge-coupled device (EMCCD) camera is implemented to image single-molecules at room temperature.

The position of a molecule is determined by localizing the center of its PSF with a Gaussian fitting (Fig. 5). The accuracy of the fitting determines the uncertainty in the localization of the fitting. Theoretically, the precision scales inversely with the square of the number of detected photons, which is described by

$$\Delta_{\text{localization}} \sim \frac{\Delta_{\text{PSF}}}{\sqrt{N}}, \tag{3}$$

where $\Delta_{\text{localization}}$ is the precision of localization, Δ_{PSF} is the width of the PSF, and N is the number of photons detected. Once $\Delta_{\text{localization}}$ is obtained, the image of the molecule can be reconstructed.

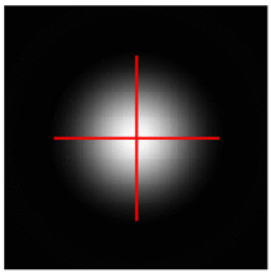

Fig. 5 Localization of one molecule with an electron-multiplying charge-coupled device (EMCCD)

Two molecules separated by a sub-diffraction distance are resolved by recording their fluorescence emission at different times (Fig. 6). The super-resolution approaches based on localization of single fluorophores are: PALM, stochastic optical reconstruction microscopy (STORM), blinking localization, Bayesian analysis of the blinking and bleaching (3B analysis), and ground state depletion microscopy followed by individual molecule return (GSDIM).

2. Photoactivated localization microscopy

PALM was first achieved by using a photoconvertible FP named EosFP (Betzig et al., 2006). PALM is based on wide-field fluorescence microscopy. The emission wavelength of the photoconvertible FPs is optically convertible from one wavelength to another. EosFP emits green fluorescence at the 516-nm wavelength. When illuminated by a beam at near the 400-nm wavelength, its emission wavelength changes to 581 nm. It is caused by a photo-induced modification involving a break in the peptide backbone next to the chromophore (Wiedenmann et al., 2004).

After a subset of EosFPs are imaged, they are photobleached, and another subset of EosFPs are converted and imaged. This process can be repeated 10^4–10^5 cycles until the population of EosFPs is depleted.

Fluorescence PALM (FPALM) uses a similar approach. It was first demonstrated using photoactivatable GFP (Hess et al., 2006).

Since 2002, a number of photoconvertible, photoactivatable, and photoswitchable FPs have been developed (Patterson et al., 2010). Photoactivatable FPs can be activated from a dark state to a bright state using UV light, and photoswitchable FPs can alternatively be switched on or off with specific illumination.

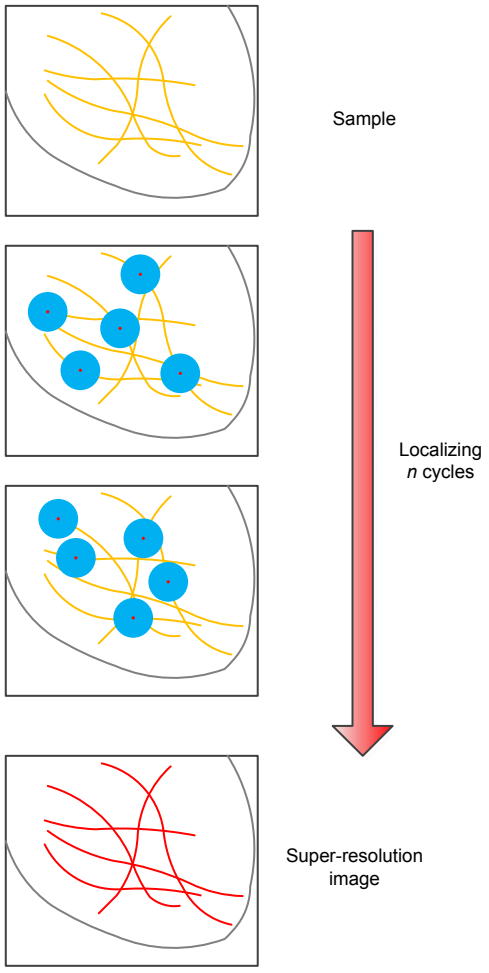

Fig. 6 Principles of photoactivated localization microscopy (PALM), stochastic optical reconstruction microscopy (STORM), blinking localization, 3B analysis, and ground state depletion microscopy followed by individual molecule return (GSDIM)

Three-dimensional FPALM was achieved in Juette et al. (2008), using biplane (BP) detection with a resolution of about 30 nm laterally and about 75 nm axially. A beam-splitter was used to split the fluorescence emission beams into a shorter and longer path to form two detection planes to determine the z-position (Juette et al., 2008).

In Shtengel et al. (2009), interferometric PALM (iPALM) provided 3D protein localization with a resolution below 20 nm. iPALM was based on single photon photoactivated localization microscopy combined with simultaneous multiphase interferometry.

3. Stochastic optical reconstruction microscopy

STORM is also based on wide-field fluorescence microscopy. It was first demonstrated using Cy3–Cy5 dye pairs (Rust et al., 2006). The Cy5 can be reversibly switched between a fluorescent and a dark state with beams at the wavelengths of 532 nm and 633 nm, respectively. The Cy3 facilitates the switching of Cy5 (Bates et al., 2005).

The optical switch can be repeated "on" and "off" hundreds or thousands of cycles before permanently bleaching the dyes. A resolution of 20 nm was demonstrated by imaging RecA-coated circular plasmid DNA (Rust et al., 2006).

Three-dimensional STORM was achieved using the astigmatism of a cylindrical lens (Huang et al., 2008a). The position of a circular fluorophore is determined by examining its elliptical image above and below the focal plane. After fitting the image with a 2D elliptical Gaussian function, the peak widths of the x and y coordinates can be obtained to calculate the z coordinate (Huang et al., 2008b).

Three-dimensional spatial resolutions of about 30 nm in the lateral direction and about 50 nm in the axial direction with the temporal resolution as fast as 1–2 s have been reported (Jones et al., 2011). Three-dimensional STORM was demonstrated by imaging microtubule networks in green monkey kidneyepithelial cells labeled with a Cy3-Alexa647 switch.

Direct STORM (dSTORM) is enabled by conventional photoswitchable fluorescent dyes. They can be reversibly switched between a fluorescent and a dark state with illumination beams at different wavelengths. dSTORM does not require special fluorophore pairs that are used in STORM. This method enables visualization of cellular structures with a resolution of approximately 20 nm without the need of an activator molecule (Vogelsang et al., 2008).

4. Blinking localization based on other emitters

PALM and STORM enable super-resolution by localizing molecules in a time sequence. These methods require at least two beams at different wavelengths.

The blinking behavior of fluorescent molecules (Cordes et al., 2010; Burnette et al., 2011), quantum dots (Lidke et al., 2005), and nitrogen-vacancy (NV) centers (Gu et al., 2013), can also be implemented in localization microscopy.

Compared with PALM and STORM, blinking localization microscopy is much simpler because it needs only one laser beam as an excitation source. The "on" state blinking fluorescence emission from single-fluorescent probes is detected by the camera of a conventional wide field microscope. The localizations are determined with a Gaussian fitting of the fluorescence intensity distributions.

5. Bayesian analysis of blinking and bleaching

3B analysis is a particularly fast method to localize fluorophores. 3B analysis builds a model arising from a number of fluorophores undergoing blinking and bleaching in the dataset and calculates the most likely distribution of fluorophore locations. It is also based on wide-field microscopy. The benefit of this method is that it can deal with images in which many fluorophores are highly overlapping, all the time, greatly reducing the number of raw images. A super-resolution image is reconstructed with a spatial resolution of 50 nm from the data collected from standard fluorescent proteins on a 4-s timescale, although the analysis requires several hours for computation (Cox et al., 2012). However, the limitation of computational cost can be improved by parallelization on cluster or cloud computing systems (Hu et al., 2013).

6. Ground state depletion microscopy followed by individual molecule return

GSDIM is based on switching the majority of the ordinary fluorophores to their triplet state T_1 or another metastable dark state and calculating the position of the fluorophores left or spontaneously returned to the ground state (Fölling et al., 2008). Transition to the long-lived triplet state with high efficiency is achieved using high-excitation intensities with an imaging buffer to obtain triplet lifetimes that are long enough so that only a subset of emitting fluorophores are left at any time in each image. The resolution of the GSDIM images is below 30 nm (Fölling et al., 2008).

GSDIM is based on wide-field microscopy and can operate with ordinary fluorophores such as organic dyes and proteins (Fölling et al., 2008; Testa

et al., 2010; Nahidiazar et al., 2016). GSDIM needs only one laser beam as an excitation source and requires recording images by camera and computer processing.

7. Minimal emission fluxes

Minimal emission fluxes (MINFLUX) is a method recently developed to reconstruct the coordinates of a molecule using minimal optical intensities (Balzarotti et al., 2017). MINFLUX is based on a confocal scanning mechanism. Compared to the other super-resolution methods, a much smaller number of detected photons N is needed to reveal the position of a molecule.

One doughnut excitation beam is implemented to provide 2D information of a molecule position. The doughnut is moved across an area of about 20 μm× 20 μm and the doughnut zero is set within 5 μs with <<1 nm precision.

The localization requires at least three coordinates of the doughnut zero, preferably arranged as an equilateral triangle. A fourth doughnut added at the center of the triangle removes ambiguities in position estimation. Therefore, the molecular location is measured with the set of localizations which are estimated with the four doughnuts (Fig. 7).

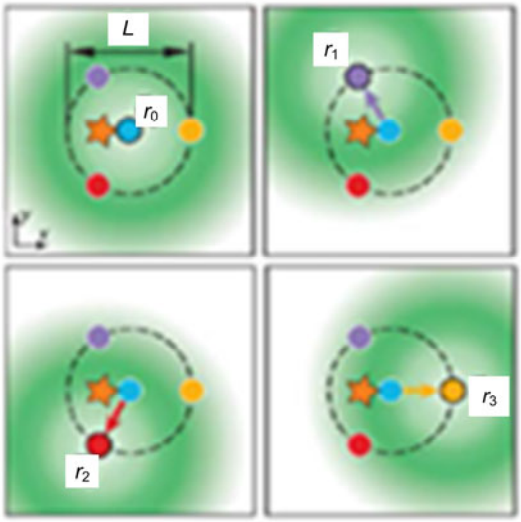

Fig. 7 Localization of one molecule with four positions
The star represents the target emitter. The four points are the central positions of the doughnuts. The fluorescent signals from these four positions are used to localize the target emitter. Reprinted from Balzarotti et al. (2017), Copyright 2017, with permission from the American Association for the Advancement of Science

Because the field of view can be moved and zoomed quickly, the setup enables fluorescence nanoscopy with short- and long-range tracking of individual emitters. MINFLUX has a 22-fold reduction of photon detections compared to methods based on localization of single fluorophores. It also attained a precision of about 1 nm, resolving molecules only 6 nm apart (Balzarotti et al., 2017). MINFLUX also enabled recording molecular trajectories with a >100-fold higher temporal resolution (Sanamrad et al., 2014).

8. Super-resolution optical fluctuation imaging

Super-resolution optical fluctuation imaging (SOFI) does not require simultaneous or sequential switching of molecules. It achieves super-resolution from temporal stochastic "on" and "off" blinking or any other stochastic intensity fluctuation. SOFI can be implemented on various microscopes: a wide-field microscope equipped with a charge-coupled device (CCD) camera, a spinning disk microscope, a scanning confocal microscope, a total internal reflection microscope, etc.

This method relies on the independent stochastic fluctuations of the emitters instead of controlled or synchronized photoactivation. It requires only taking a movie of the sample (Fig. 8).

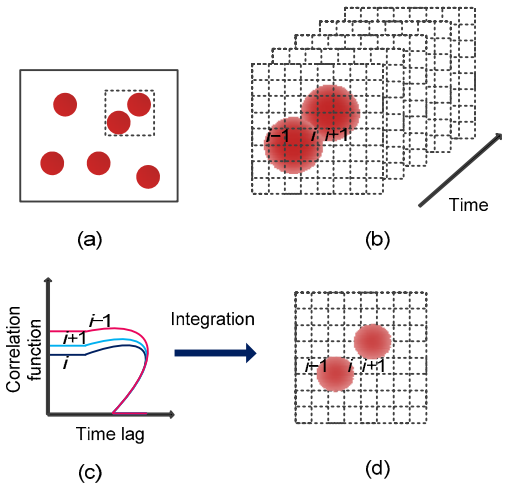

Fig. 8 Principle of super-resolution optical fluctuation imaging (SOFI): (a) wide-field imaging; (b) a movie recoding two fluorescent probes in three neighboring pixels; (c) second-order correlation function calculated for each pixel; (d) SOFI intensity value for each pixel

The signal in a pixel is given by the superposition of the fluorescence signals from different

fluorescent probes. Each pixel value of an SOFI image (of the order n) is obtained from the n^{th}-order cumulant of the original pixel time series. The n^{th}-order cumulant filters the signals based on their fluctuations in such a way that only highly correlated fluctuations remain.

Because the remitting signal is limited to emitters within the pixel, the fluorescence signal contribution of these emitters to neighboring pixels nonlinearly yields lower correlation values. Super-resolution is achieved by subtracting the n^{th}-order cumulant with a correlation calculation. A 5-fold improvement in spatial resolution was demonstrated with a wide-field microscope (Dertinger et al., 2009).

Since SOFI is totally software based, compared with previous super-resolution methods, it shows several advantages such as simplicity, affordability, high speed, and low levels of light exposure (Dertinger et al., 2012).

2.2 Non-fluorescence-based super-resolution

2.2.1 Hyperlenses and metalenses for far-field super-resolution imaging

1. Principle of hyperlens

The light emitted or scattered from objects includes propagating and evanescent components. The propagating waves with low wave-vectors carry low-frequency information and can reach the far field. However, the evanescent waves with high wave-vectors carry high-frequency information and are obstructed in the near field in a normal material environment. Thus, high-frequency information cannot contribute to the final image in the far field, leading to the diffraction barrier.

Two conditions are required to achieve super-resolution with a hyperlens: a material that allows propagating waves with high wave-vectors, and a magnification mechanism that converts the high wave-vector waves into low wave-vector waves, allowing the high-frequency information to reach the far field.

Anisotropic plasmonic metamaterials provide one practical option. The overall loss in plasmonic metamaterials is reduced because only permittivities along different directions need to be designed (Podolskiy et al., 2005; Yao et al., 2008). The simplest anisotropic plasmonic metamaterials can be constructed by the deposition of alternating metal or dielectric multilayers.

When the layer thickness is much smaller than the working wavelength, an effective-medium approximation is commonly used to describe the permittivities along different directions. Unlike isotropic media with a spherical dispersion, the dispersion properties for multilayer metamaterials can be designed to have $\varepsilon_x' > 0$ and $\varepsilon_z' < 0$ for hyperbolic dispersions or $\varepsilon_z' \gg \varepsilon_x' > 0$ for eccentric elliptic dispersions, where ε_x' and ε_z' are the real parts of the permittivity along the x and z directions.

Anisotropic metamaterials with unbounded wave-vector values or very large wave-vector cut-off support the propagation of high wave-vectors. The working wavelength for multilayer metamaterials can be tuned across a broad band of wavelengths with combinations of different materials.

The magnification mechanism is that the wave-vector compression can be achieved by bending the flat layers into co-centrically curved layers (Jacob et al., 2006; Zhang and Liu, 2008).

A number of practical hyperlenses have been proposed, including a cylindrical geometry (Pendry and Ramakrishna, 2002; Jacob et al., 2006), tapered metallic wire arrays (Ono et al., 2005; Ikonen et al., 2007; Shvets et al., 2007; Zhao et al., 2010), or uniquely designed material dispersions (Han et al., 2008; Kildishev and Shalaev, 2008; Tsang and Psaltis, 2008; Li LJ et al., 2009).

The first one-dimensional optical hyperlens was demonstrated at an ultraviolet wavelength with a resolution of 130 nm (Liu et al., 2007). It was created by conformal deposition of Ag and Al_2O_3 multilayer films on a cylindrical quartz cavity. In other experimental results, a hyperlens achieved 125-nm resolution (λ/2.92) at the 365-nm working wavelength (Xiong et al., 2009). Despite all this, some simulations predicted a much higher resolution around λ/9 (Xiong et al., 2009).

The 2D hyperlens achieved the 205-nm resolution (λ/2) at the 410-nm working wavelength (Rho et al., 2010). It was created by deposition of alternating layers of Ag and Ti_3O_5 thin films in a hemispherical geometry designed with hyperbolic dispersion.

2. Principle of metalenses

A metalens is based on a metamaterial slab with phase compensation, which makes a plane wave focus.

Anisotropic metamaterials with either a hyperbolic or eccentric elliptic dispersion support the propagation of high-frequency information. Therefore, the metalens has the same material requirement as the hyperlens, such as multilayers (Liu et al., 2007) and nanowire metamaterials (Yao et al., 2008).

The high wave-vector waves are totally reflected at the interface between metamaterial and air. Therefore, a bidirectional coupler is required to convert waves from high wave-vectors in the metamaterial to low wave-vectors in air. In addition, this coupler needs the focusing function enabled by phase compensation (Ma and Liu, 2010b; Ma et al., 2011).

The phase matching condition needs to be satisfied to make plane waves from air focus inside the metamaterial. This can be achieved by either geometric variations, such as plasmonic waveguide couplers (PWC) (Sun and Kim, 2004; Verslegers et al., 2009a; Ma and Liu, 2010b; Ma et al., 2011) and shaped metamaterial-air interfaces (Parazzoli et al., 2004; Ma and Liu, 2010a), or material refractive-index variations, such as gradient-index (GRIN) metamaterials (Verslegers et al., 2009b; Ma et al., 2011).

The metalens with an elliptic dispersion obtained a focal spot with a full width at half maximum of 59 nm (about λ/6.2) at ultraviolet wavelengths (Ma and Liu, 2010b). An improved resolution (about λ/8.6) was proved at longer wavelengths, due to smaller material loss (Ma and Liu, 2011). A 70-nm (about λ/9) focal spot was formed at a focal length of 3 mm for normal plane-wave incidence at 633 nm (Ma and Liu, 2010a).

2.2.2 Microsphere-based super-resolution imaging

Super-resolution imaging can also be achieved by using dielectric microspheres (Wang et al., 2011; Darafsheh et al., 2012, 2014; Darafsheh, 2013; Li et al., 2013; Yang et al., 2014; Astratov and Darafsheh, 2017). The super-resolution capability of spheres results from their extraordinarily sharp focusing properties, so-called "photonic nanojets" (Chen et al., 2004; Ferrand et al., 2008). Spheres are placed closer to the sample than solid immersion lenses (Lee JY et al., 2009; Mason et al., 2010; Kim et al., 2011) because of smaller contact regions. A virtual image with fine sample details is obtained with microsphere capability and can be collected by confocal microscopes (Fig. 9).

At first, this technique was developed with silica spheres with n about 1.46 and diameter D about 2–9 μm (Wang et al., 2011). Later, it was demonstrated (Darafsheh et al., 2012, 2014; Darafsheh, 2013; Yang et al., 2016; Astratov and Darafsheh, 2017) that high index (n≈1.9–2.1) and total liquid immersion enabled imaging with a resolution of about λ/7–λ/6.

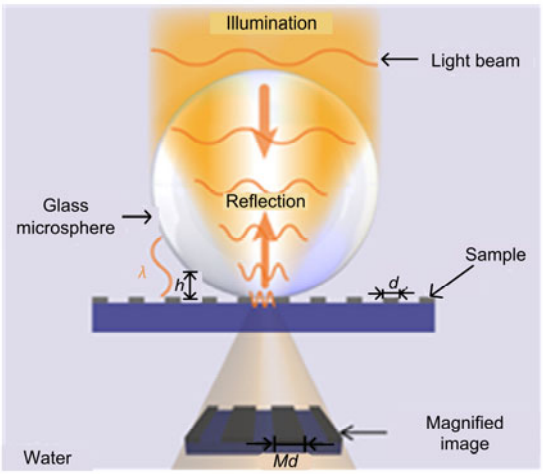

Fig. 9 Super-resolution imaging with a dielectric microsphere

One dielectric microsphere is placed on a grating (line width is d) and illuminated from the front. The reflected light from the grating allows detection of a magnified virtual image (magnification factor is M). When the distance h between the microsphere and the grating is small enough (of order of the illumination wavelength λ), the near-field evanescent wave carrying the high-frequency information begins propagating in the high refractive-index sphere, and is then collected by the microscope objective. Reprinted from Yang et al. (2016), Copyright 2016, with permission from American Chemical Society

3 Highlighted achievement

3.1 Multicolor imaging

Multicolor microscopy allows us to understand the functionality of different biological structures by imaging them with a broad range of wavelengths. The accuracy of colocalization of different fluorescent labels is limited by the resolution of the implemented imaging method. Multicolor super-resolution imaging provides a better understanding of molecular interactions in cells at the nanoscale.

Multicolor STED can be achieved using fluorophores with different excitation and emission

wavelengths. Two-color STED was demonstrated with green and red fluorescent beads (excitation at 488-nm wavelength and STED at 603-nm wavelength for Atto 532; excitation at 635-nm wavelength and STED at 750–780 nm wavelengths for Atto 647N) (Donnert et al., 2007).

Another approach for multicolor STED imaging is to use fluorescent dyes with very large Stokes shifts. Two fluorophores with different excitation wavelengths are resolved by depleting their fluorescence with the same STED beam. Images of the mitochondrial outer membrane and a matrix in three dimensions were achieved with DY-485XL and NK51 excited at 488 nm and 532 nm, respectively (Schmidt et al., 2008).

The same concept has recently been extended up to three (Galiani et al., 2016; Sidenstein et al., 2016) and four (Winter et al., 2017) fluorophores. Four-color STED imaging is shown in Fig. 10. New fluorophores with a long Stokes shift may boost the multicolor ability of STED microscopy (Sednev et al., 2015).

Furthermore, another multicolor STED method requires rigorous linear unmixing algorithms to distinguish two fluorophores when a single excitation and STED beams are implemented for imaging (Tønnesen et al., 2011; Lukinavičius et al., 2016).

Multicolor STORM was demonstrated in imaging microtubules with clathrin-coated pits involved in receptor-mediated endocytosis (Bates et al., 2005). The microtubules and clathrin were labeled by Cy2-Alexa647 and Cy3-Alexa647, respectively. Laser beams at the wavelengths of 457 nm and 532 nm respectively, were used to selectively excite fluorescence. Microtubules were imaged separately from the circular clathrin pits with a spatial resolution of about 30 nm. Two-color STORM was also demonstrated in super-resolution imaging of mitochondria (Huang et al., 2008).

New switchable rhodamine dyes with the same activation but different emission wavelengths were proposed for three-color imaging of fluorescent microspheres and two-color imaging of microtubules (Bossi et al., 2008).

Three-dimensional multicolor STORM (up to three-color) was applied to trace neural connectivities in the hippocampal region (Lakadamyali et al., 2012). The organization of actin, spectrin, and associated proteins in neurons was studied with two-color STORM (Fig. 11) (Xu et al., 2013).

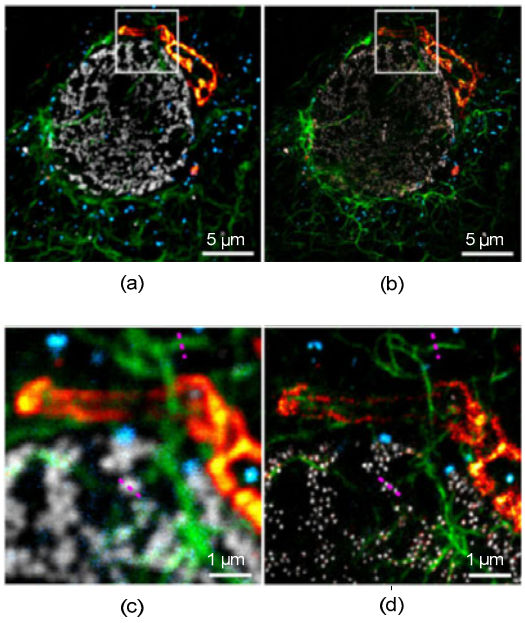

Fig. 10 Four-color stimulated emission depletion (STED) imaging of a fixed cell: (a) confocal overlay; (b) STED overlay; (c) enlarged view of the region in the white square in (a); (d) enlarged view of the region in the white square in (b)

Excitation wavelength is 612 nm; STED wavelength is 775 nm. The fluorescence is detected by a hyperspectral detection design spanning a total range of 620–750 nm in four channels (blue: peroxisomes–Atto594; green: vimentin–Abberior Star635P; red hot: giantin–KK1441; grey: nuclear pores–CF680R) (Winter et al. (2017), licensed under CC BY 4.0). References to color refer to the online version of this figure

Two-color PALM was demonstrated by imaging COS-7 cells with PAmCherry1 and PA-green fluorescent protein (PAGFP) (Subach et al., 2009). Laser beam at 561-nm and 468-nm wavelengths were used to excite the red (PAmCherry1) and green (PAGFP) dyes, respectively.

Two-color GSDIM was demonstrated in imaging of microtubules and peroxisomes in PtK2-cells labeled by rhodamine and fluorescent proteins (Fölling et al., 2008). Three-color GSDIM was employed in imaging of F-actin, clathrin, and tubulin in fixed PtK2 cells with a resolution of 15 nm (Testa et al., 2010).

3.2 Live-cell imaging

Although the electron microscopy provides a much higher resolution than conventional optical

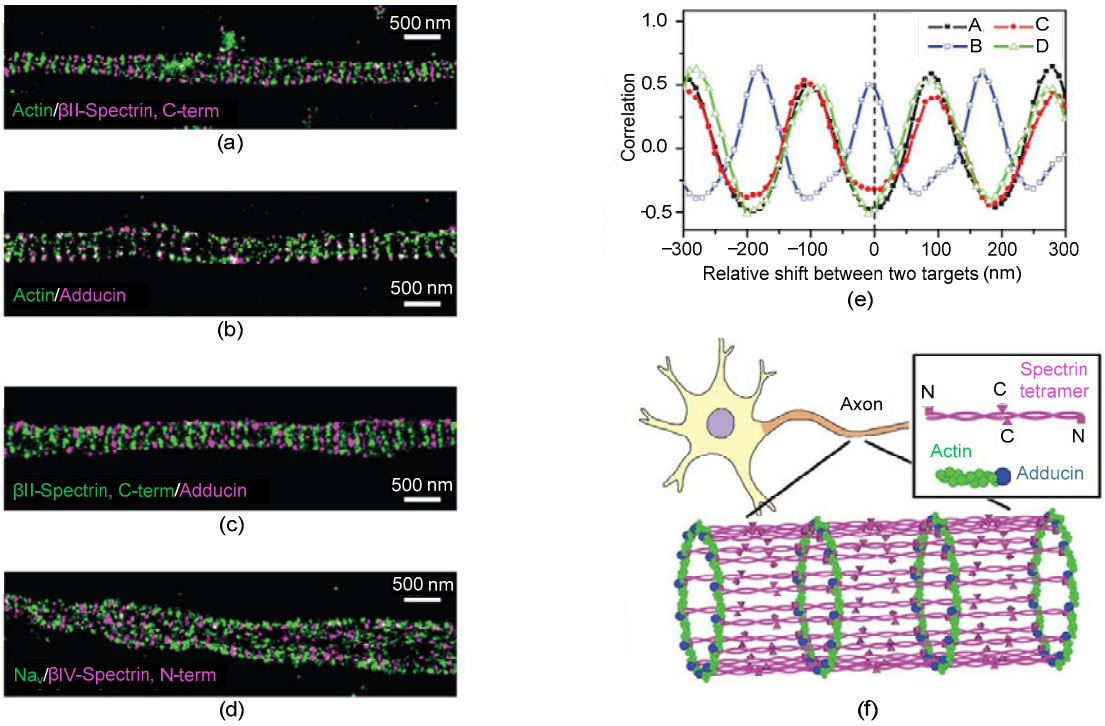

Fig. 11 Two-color STORM imaging of actin, spectrin, adducin, and sodium channels: (a) two-color STORM image of actin (green) and βII-spectrin (magenta); (b) two-color STORM image of actin (green) and adducin (magenta); (c) two-color STORM image of βII-spectrin (green) and adducin (magenta); (d) two-color STORM image of sodium channels (Na$_v$, green) and βIV-spectrin (magenta); (e) spatial correlations between actin and the βII-spectrin C terminus [(A), black], between actin and adducin [(B), blue], between adducin and the βII-spectrin C terminus [(C), red], and between sodium channels and the βIV-spectrin N terminus [(D), green]; (f) a model for the cortical cytoskeleton in axons

βII-spectrin is immunostained against its C-terminal region, which is situated at the center of the spectrin tetramer. βIV-spectrin is immunostained against its N-terminal region, which is situated at the two ends of the spectrin tetramer. Short actin filaments (green), capped by adducin (blue) at one end, form ringlike structures wrapping around the circumference of the axon. Spectrin tetramers (magenta) connect the adjacent actin/adducin rings along the axon, creating a quasi-1D lattice structure with a periodicity of about 180 to 190 nm. Reprinted from Xu et al. (2013), Copyright 2013, with permission from the American Association for the Advancement of Science. References to color refer to the online version of this figure

microscopy, the samples require coating and cannot be alive. On the other hand, super-resolution fluorescence microscopy can still image live cells with a very high resolution.

SIM is a popular choice for live-cell imaging due to its high acquisition speed and no special requirements for fluorophores.

SIM was applied to image living cells with the volume rates of 4 s in one color and 8.5 s in two colors (Fiolka et al., 2012). It was enabled by fast programmable liquid crystal devices and a flexible 2D grid pattern algorithm to switch between excitation wavelengths.

High-speed SIM was demonstrated to image tubulin and kinesin dynamics in living cells at frame rates up to 11 frames/s (Hirvonen et al., 2009; Kner et al., 2009). SIM enabled imaging of the process of DNA break repair (Fig. 12) (Lesterlin et al., 2014) and the cytoskeleton in adherent cells (Burnette et al., 2014).

STED nanoscopy was also implemented to image live cells by increasing the scanning speed and limiting the field of view. A video-rate (28 frames/s) imaging of live hippocampal neurons showing the movement of individual synaptic vesicles with a 60–80 nm resolution was demonstrated (Westphal et al., 2008). Live cells STED imaging was also demonstrated with the acquisition time of about 8 s using standard fluorescent proteins (Rankin et al., 2011).

Moreover, STED enabled in vivo imaging of enhanced yellow fluorescent proteins (eYFP) in neurons as deep as 15 μm into the brain of a mouse (Fig. 13) (Berning et al., 2012). STED was also applied to image living cells with fluorescent rhodamines and fluorogenic carbopyronines (Butkevich et al., 2016). Cytoskeleton features were revealed with STED in living neurons (D'Este et al., 2015).

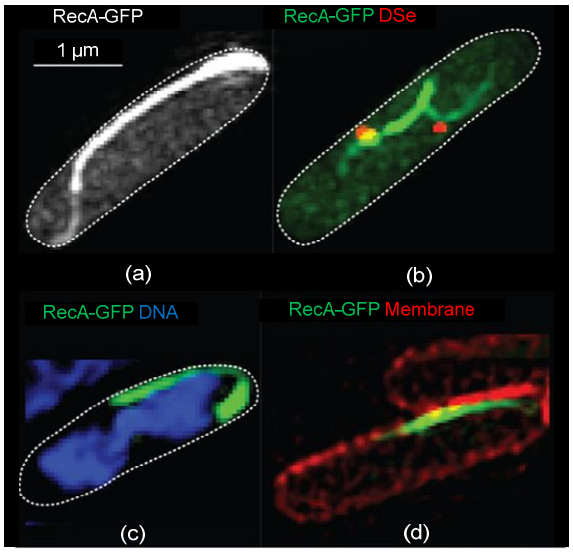

Fig. 12 Three-dimensional structured-illumination microscopy (SIM) of cells with DSB-induced RecA-GFP bundles alone (a), with DSe foci (b), relative to DNA (c), and relative to membrane (d). Reprinted from Lesterlin et al. (2014), Copyright 2013, with permission from Springer Nature

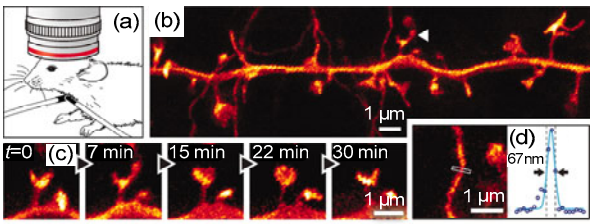

Fig. 13 STED imaging of neurons in a mouse brain: (a) anesthetized mouse under the objective lens with tracheal tube; (b) projected volumes of dendritic and axonal structures reveal; (c) temporal dynamics of spine morphology; (d) an improved resolution of 67 nm. Reprinted from Berning et al. (2012), Copyright 2012, with permission from the American Association for the Advancement of Science

Fluorescent proteins required for PALM are already commonly implemented to image living cells. Super-resolution imaging of adhesion proteins in live cells with PALM was demonstrated with spatial resolutions down to about 60 nm and a frame duration of 25 s (Shroff et al., 2008). Photoswitchable eYFP-labeled live bacteria enabled super-resolution imaging of the MreB structure in cells (Biteen et al., 2008).

STORM achieved live-cell imaging with a spatial resolution of about 25 nm and a temporal resolution of 0.5 s in two dimensions (Jones et al., 2011). Cells were labeled with proteins directly or via SNAP-tags with fast photo-switchable dyes.

A spontaneously blinking fluorophore enabled repetitive time-lapse super-resolution imaging of microtubules in live cells for 1 h (Uno et al., 2014). The blinking was based on an intramolecular spirocyclization reaction.

GSDIM was applied to image living PtK2 cells labeled with the organic dye TMR via an SNAP tag or with the fluorescent protein Citrine (Testa et al., 2010).

The SOFI method was also applied to image the 3D network of mitochondria in fixed C2C12 cells and the 3D vimentin structure in living Hela cells (Geissbuehler et al., 2014).

3.3 Significant enhancement of resolution

Spatial resolution in STED nanoscopy strongly relies on the photostability of the sample.

Negatively charged nitrogen vacancy (NV^-) centers are fluorescent probes with outstanding photostability and no photobleaching. They can tolerate a huge number of excitation/STED cycles, with transitions to the dark singlet state nearly absent. Therefore, they are well suited for STED imaging. The highest resolution reported with STED imaging (down to 5.8 nm) was achieved with NV^- centers (Rittweger et al., 2009a).

STED of biological samples enabled imaging with a resolution of 50–100 nm without causing significant photodamage (Westphal et al., 2008; D'Este et al., 2015; Butkevich et al., 2016).

In addition, GSD nanoscopy with NV^- centers provided an extremely high resolution of 7.8 nm (Rittweger et al., 2009b).

The resolution of PALM, STORM, GSDIM, and blinking localization methods is determined by the number of detected photons, as mentioned above. In theory, a resolution of 10 nm is possible with about

1000 photons, but in practice a resolution of about 20 nm with 6000 photons is quite common due to the mechanical drift and the error of Gaussian fitting (Betzig et al., 2006; Rust et al., 2006).

4 Instrumentation

The development and commercialization of super-resolution microscopes based on SIM, STED, STORM, and PALM are rapidly progressing. The specifications of the latest super-resolution commercial microscopes are reported in Tables 1–4.

SIM microscopes are produced by Nikon (Nikon, Tokyo, Japan), Zeiss (Zeiss, Jena, Germany), and Olympus (Olympus, Tokyo, Japan) (Table 1). The N-SIM system has a better lateral resolution and can provide up to five color channels. The SpinSR10 system is based on a spinning disk confocal microscope. Thus, the acquisition speed is 200 times higher than those of N-SIM and ELYRA S.1 microscopes, which are based on wide-field modality. Besides, ELYRA S.1 can be combined with ELYRA P.1, which is based on the PALM technology. Two methods of super-resolution imaging, SIM and PALM, can be provided in one system.

The microscopes currently available for STED imaging are Leica TCS SP8 (Leica Microsystems, Wetzlar, Germany) and different products from Abberior (Abberior, Göttingen, Germany) (not restricted in Table 2). The 775 STED system can achieve the highest lateral resolution up to 20 nm, while Easy3D

Table 1 Specifications of microscopes based on structured-illumination microscopy (SIM)

Company	Product	Lateral resolution (nm)	Axial resolution (nm)	Acquisition speed	Camera	Number of colors
Nikon	N-SIM	85–115	300	0.6–1.0 s/frame (1–2 s for calculation)	EMCCD	5
Zeiss	ELYRA S.1	120	300	1.5–1.6 s/frame	EMCCD	2
Olympus	SpinSR10	120	X	5 ms/frame	CMOS	2

Table 2 Specifications of microscopes based on stimulated emission depletion (STED)

Company	Product	Lateral resolution (nm)	Axial resolution (nm)	STED wavelength (nm)	Excitation wavelength (nm)	Number of colors
Leica	Leica TCS SP8	30–80	130	592, 660, 775	Up to 8 wavelengths	5
Abberior	775 STED	20–30	Confocal	775	594, 640	2
Abberior	595 STED	25–40	Confocal	595	488, 518	2
Abberior	Easy3D STED	75–100	75–100	775	594, 640	3

Table 3 Specifications of microscopes based on stochastic optical reconstruction microscopy (STORM), photoactivated localization microscopy (PALM), and ground state depletion microscopy followed by individual molecule return (GSDIM)

Company	Product	Lateral resolution (nm)	Axial resolution (nm)	Maximum field of view (μm)	Acquisition speed	Camera	Number of colors
Bruker	Vutara 352	20	50	40×40	Up to 3000 frames/s	sCMOS	2
ONI	Nanoimager	20	50	50×80	100 frames/s for full frame and 5 kHz with frame height cropped to 2%	sCMOS	2
Nikon	N-STORM 5.0	20	50	80×80	Up to 500 Hz	sCMOS	3
Zeiss	ELYRA P.1	20	50–80	81.1×81.1	30 frames/s for full frame and >100 frames/s in sub-array mode	EMCCD	3
Leica	Leica SR GSD 3D	20	50	40×40	Over 1000 frames/s	sCMOS	3

Table 4 Specifications of microscopes based on reversible saturable optically linear fluorescence transitions (RESOLFT)

Company	Product	Lateral resolution (nm)	Optical system	Doughnut number	Number of colors
Abberior	RESOLFT	<70	Point scanning	1	2
Abberior	2-color RESOLFT parallel	<80	Wide-field	>100 000	2

STED can obtain a 3D resolution of 75 nm. Leica TCS SP8 provides more options with up to eight channels for the excitation pulsed laser beams. It also enables simultaneously recording up to five different emission wavelengths.

STORM and PALM microscopes include four products, Vutara 352 from Bruker (Bruker, Massachusetts, USA), Nanoimager from Oxford Nanoimaging (Oxford Nanoimaging, Oxford, UK), N-STORM 5.0 from Nikon, and ELYRA P.1 from Zeiss (Table 3). The four systems show the same resolution in lateral and axial directions. N-STORM 5.0 and ELYRA P.1 can provide a large field of view and support three-color imaging. Nanoimager has the highest acquisition speed, and Leica SR GSD 3D (Leica Microsystems, Wetzlar, Germany), based on GSDIM, shows specifications similar to the four systems above, but can be used for a wide range of fluorophores.

Two types of RESOLFT microscopes from Abberior are shown in Table 4. The RESOLFT point scanning system equipped with Abberior QUAD scanner with four galvo mirrors can obtain a scanning line frequency of 2 kHz. The two-color RESOLFT parallel system also achieves a high acquisition speed with fast sCMOS cameras.

5 Other applications

5.1 Three-dimensional sub-diffraction optical laser lithography

Although electron beam lithography (Rai-Choudhury, 1997), or plasmonic lithography (Pan et al., 2011), provides nanometer resolution, these techniques can be used for only 2D nanofabrication. Three-dimensional optical laser lithography, also called 3D direct laser writing (DLW), has enabled nanofabrication in three dimensions.

In 3D DLW, a pulsed laser is typically focused into a diffraction-limited spot within the volume of a photoresist. The photoresist is exposed within this volume by exploiting two-photon absorption and/or other optical nonlinearities. An improvement in the resolution of 3D DLW is achieved by decreasing the lateral and/or the axial size of the exposed volume with controlled exposure. However, the resolution of the 3D DLW process is still limited by the diffraction barriers.

Because the STED concept was introduced in fluorescence microscopy, similar ideas based on super-resolution photoinduction/inhibition nanolithography (SPIN) have been applied in 3D DLW lithography (Li LJ et al., 2009; Scott et al., 2009; Fischer et al., 2010; Cao et al., 2011; Fischer and Wegener, 2011; Gan et al., 2013).

In a regular DLW process, the photoresist is excited by a laser, eventually inducing an irreversible chemical reaction, such as polymerization. For common negative-tone photoresist, the exposed regions become insoluble, whereas the unexposed regions can be removed during development treatment.

SPIN methods are taking advantage of inhibiting some intermediate states to reduce the size of the excited and exposed photoresist. The inhibition is induced by a second laser generally at a different wavelength from the excitation beam. Three SPIN techniques have been developed, which are discussed below (Fig. 14).

In SPIN based on photoluminescence (Fischer et al., 2010; Fischer and Wegener, 2011), photo-initiator molecules are excited through two-photon absorption. After relaxing to the S_1 state, they are brought back to the ground state through stimulated emission and then proceed to the triplet (T_1) through intersystem crossing. The process generates radicals, initiates a propagation polymer chain, and finally brings an irreversibly cross-linked polymer.

In SPIN through photodeactivation (Li LJ et al., 2009), photo-initiator molecules are excited through two-photon absorption and yield an active species in an intermediate state with a long lifetime. Once the light beam excites the molecules, the intermediate state is deactivated and does not lead to cross-linking polymerization.

In SPIN through photoradical generation (Scott et al., 2009; Cao et al., 2011; Gan et al., 2013), photo-initiator molecules are excited through one- or two-photon absorption at different wavelengths, generating radicals that can initiate the polymerization. Photo-inhibitor molecules are activated through one- or two-photon absorption at a different wavelength. The generated non-initiating radicals can clean initiating radicals and stop propagating chains.

The three described principles are enabled for sub-wavelength DLW to print structures with much

smaller features. The experimental results of super-resolution DLW are shown in Table 5. The up-to-date smallest feature size (9 nm) and line resolution (52 nm) have been achieved by 2PII lithography and two-photon absorption (Gan et al., 2013).

3D sub-diffraction DLW has provided a powerful tool for complex 3D nanofabrication and 3D data storage (Grotjohann et al., 2011).

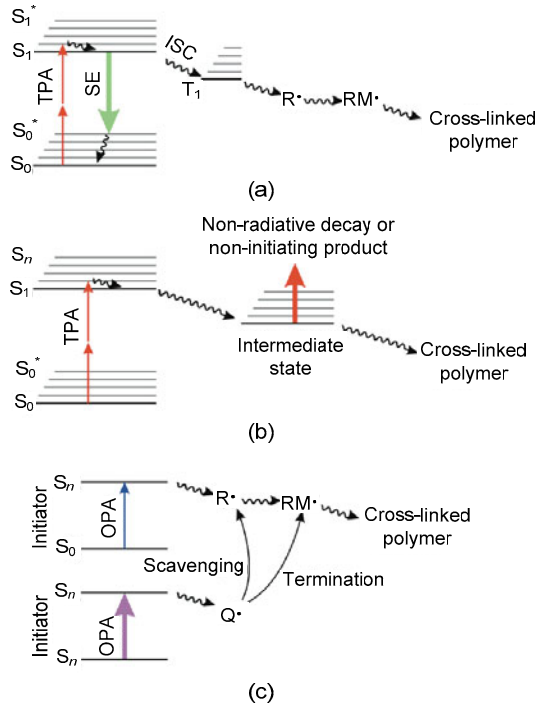

Fig. 14 Depletion principle: (a) photoluminescence; (b) photodeactivation; (c) photoradical generation

It is noted that photoradical generation can be applied with not only one-photon absorption (OPA) but also two-photon absorption (TPA). SE: stimulated emission; ISC: through intersystem crossing; R: radicals; RM: propagation polymer chain; Q: non-initiating radicals (Fischer and Wegener (2013), licensed under CC BY 4.0)

Table 5 Results of super-resolution direct laser writing (DLW)

Year	Principle	Resolution (nm)	Lateral (nm)	Axial (nm)
2009	Photodeactivation	X	X	40 (D)
2009	Photoradical	X	110 (D)	X
2010	Photoluminescence	X	65 (L)	X
2011	Photoluminescence	175	X	170 (L)
2011	Photoradical	X	40 (D) 130 (L)	X
2013	Photoradical	52	9 (L)	32 (L)

D: dots; L: line; X: not known

5.2 Magnetic imaging

Magnetic imaging applied to life science can provide new information of biological functions. The study of action potentials propagation along neurons has recently attracted wide interest (Barry et al., 2016; Hortigon-Vinagre et al., 2016). Furthermore, a magnetic protein responsible for migration and orientation in animals has recently been discovered (Qin et al., 2016).

However, current techniques cannot provide a high magnetic imaging resolution at room temperature. Some techniques such as magnetic resonance imaging (Lee SC et al., 2009) have low spatial resolution (1–5 μm) compared to optical microscopy. Therefore, magnetic resonance imaging is not generally applicable to image sub-cellular structures.

Other techniques that enable magnetic field measurements are scanning superconducting quantum interference device microscopy (Finkler et al., 2010), electron holography (Dunin-Borkowski et al., 1998), and magnetic resonance force microscopy (Degen et al., 2009). These methods provide a sub-micrometer resolution but require operating conditions that restrict application to living biological samples.

NV^- centers provide magnetic imaging via optically detected magnetic resonance (ODMR) with a high spatial resolution at room temperature (Gruber et al., 1997). An NV^- center is excited at the 532-nm wavelength and emits broadband photoluminescence with zero photon line at the 637-nm wavelength (Gruber et al., 1997). The NV^- center has a spin-triplet ground state with a zero-field splitting of about 2.87 GHz between the m_s=0 and m_s=±1 spin states (Pham et al., 2011).

When NV^- centers are stimulated by a microwave field, redistribution might occur in the population of the electrons of NV^- centers in the ground state. When the microwave frequency is switched to the zero-field splitting frequency (2.87 GHz), m_s=±1 states become more populated and the m_s=0 state becomes less populated (Gruber et al., 1997). Therefore, this leads to a photoluminescence decrease (ODMR signal) because of the non-radiative decay via the intermediate metastable state.

If a magnetic field is also applied, the m_s=−1 and m_s=+1 states split and the gap increases proportionally

with the strength of the magnetic field. The application of a microwave field and a magnetic field leads to an increase in the population of the m_s=−1 and m_s=+1 states. The ODMR signal shows two dips because of the electron redistribution. The distance between the two dips increases with the strength of the magnetic field applied.

Magnetic imaging with micron scale resolution via ODMR has been achieved in living magnetotactic bacteria (Le et al., 2013), tumor cells (Glenn et al., 2015), and mammalian cells (Davis et al., 2018). Magnetic imaging with nanoscale resolution needs to spatially assign the spin of the NV^- center at nanoscale as a precondition.

In bulk diamond, super-resolution microscopy combined with spin assignment has been demonstrated with charge-state depletion (CSD) (Chen et al., 2015), STORM (Chen et al., 2015), and RESOLFT (Jaskula et al., 2017). A spatial resolution of 4.1 nm with CSD has been achieved. In nanodiamonds, two collectively blinking NV^- centers separated by a distance of 23 nm were resolved using blinking localization microscopy with ODMR (Barbiero et al., 2017).

6 Conclusions

In this paper, we reviewed the principles of various super-resolution microscopes, including fluorescence- and non-fluorescence-based methods. The fluorescence-based super-resolution microscopes were divided into two main categories, spatial-domain methods (SIM, SSIM, STED, and RESOLFT) and time-domain methods (PALM, STORM, blinking localization, MINFLUX, and SOFI).

Except for SIM, ISM, and MINFLUX, all the fluorescence-based super-resolution microscopy methods take great advantage of special properties of fluorescent probes. A huge enhancement of spatial resolution is achieved by distinguishing the fluorescent probes in two different states, “on” and “off.” The “on” state can provide the desired fluorescence, while the “off” state cannot due to various mechanisms. On the other hand, special material technologies are applied to achieve super-resolution with non-fluorescence-based methods.

In general, the resolution obtained by fluorescence-based super-resolution techniques is better than that obtained by non-fluorescence-based ones. Furthermore, a number of achievements of fluorescence-based imaging methods, such as multicolor imaging and live-cell imaging, were presented. Fluorescence-based super-resolution has already led to a revolution in biological imaging, boosting the study in various biology fields. The non-fluorescence-based super-resolution methods have no special requirements for samples. Therefore, they might have broader application prospects.

We also presented the status of instrumentation of super-resolution microscopes and compared the specifications of the commercial products. Super-resolution methods have a potential application in improving the resolution of in vivo endoscopic imaging, which is limited by the low numerical aperture (NA). The STED principle was applied in a two-photon endoscope to obtain a resolution of 310 nm, which broke the diffraction limit by a factor of three (Gu et al., 2014).

Inspired by super-resolution methods in STED microscopy, three SPIN methods were developed and enabled 3D nanofabrication with application in optical data storage (Grotjohann et al., 2011; Gu et al., 2016).

Super-resolution optical magnetic imaging is also very promising as a new tool for understanding biological processes. Nanoscale magnetic imaging with NV^- centers in NDs requires spatially assigning the spin at nanoscale. Non-invasive nanoscale magnetic mapping of biological samples represents a promising application for the next generation super-resolution microscopes.

References

Abbe E, 1873. Beiträge zur theorie des mikroskops und der mikroskopischen wahrnehmung. *Arch Mikrosk Anat*, 9(1):413-418. https://doi.org/10.1007/BF02956173

Astratov VN, Darafsheh A, 2017. Methods and Systems for Super-resolution Optical Imaging Using High-Index of Refraction Microspheres and Microcylinders. University of North Carolina at Charlotte, Charlotte, NC, USA.

Azuma T, Kei T, 2015. Super-resolution spinning-disk confocal microscopy using optical photon reassignment. *Opt Expr*, 23(11):15003-15011. https://doi.org/10.1364/OE.23.015003

Balzarotti F, Eilers Y, Gwosch KC, et al., 2017. Nanometer resolution imaging and tracking of fluorescent molecules with minimal photon fluxes. *Science*, 355(6325):606-612.

https://doi.org/10.1126/science.aak9913

Barbiero M, Castelletto S, Gan XS, et al., 2017. Spin-manipulated nanoscopy for single nitrogen-vacancy center localizations in nanodiamonds. *Light Sci Appl*, 6(11):e17085. https://doi.org/10.1038/lsa.2017.85

Barry JF, Turner MJ, Schloss JM, et al., 2016. Optical magnetic detection of single-neuron action potentials using quantum defects in diamond. *Proc Nat Acad Sci USA*, 113(49):14133-14138. https://doi.org/10.1073/pnas.1601513113

Bates M, Blosser TR, Zhuang XW, 2005. Short-range spectroscopic ruler based on a single-molecule optical switch. *Phys Rev Lett*, 94(10):108101. https://doi.org/10.1103/PhysRevLett.94.108101

Berning S, Willig KI, Steffens H, et al., 2012. Nanoscopy in a living mouse brain. *Science*, 335(6068):551. https://doi.org/10.1126/science.1215369

Betzig E, 1995. Proposed method for molecular optical imaging. *Opt Lett*, 20(3):237-239. https://doi.org/10.1364/OL.20.000237

Betzig E, Patterson GH, Sougrat R, et al., 2006. Imaging intracellular fluorescent proteins at nanometer resolution. *Science*, 313(5793):1642-1645. https://doi.org/10.1126/science.1127344

Biteen JS, Thompson MA, Tselentis NK, et al., 2008. Super-resolution imaging in live *Caulobacter crescentus* cells using photoswitchable EYFP. *Nat Methods*, 5(11):947-949. https://doi.org/10.1038/nmeth.1258

Böhm U, Hell SW, Schmidt R, 2016. 4Pi-RESOLFT nanoscopy. *Nat Commun*, 7:10504. https://doi.org/10.1038/ncomms10504

Bossi M, Fölling J, Belov VN, et al., 2008. Multicolor far-field fluorescence nanoscopy through isolated detection of distinct molecular species. *Nano Lett*, 8(8):2463-2468. https://doi.org/10.1021/nl801471d

Bretschneider S, Eggeling C, Hell SW, 2007. Breaking the diffraction barrier in fluorescence microscopy by optical shelving. *Phys Rev Lett*, 98(21):218103. https://doi.org/10.1103/PhysRevLett.98.218103

Burnette DT, Sengupta P, Dai YH, et al., 2011. Bleaching/blinking assisted localization microscopy for superresolution imaging using standard fluorescent molecules. *Proc Nat Acad Sci USA*, 108(52):21081-21086. https://doi.org/10.1073/pnas.1117430109

Burnette DT, Shao L, Ott C, et al., 2014. A contractile and counterbalancing adhesion system controls the 3D shape of crawling cells. *J Cell Biol*, 205(1):83-96. https://doi.org/10.1083/jcb.201311104

Butkevich AN, Mitronova GY, Sidenstein SC, et al., 2016. Fluorescent rhodamines and fluorogenic carbopyronines for super‐resolution STED microscopy in living cells. *Angew Chem Int Ed*, 55(10):3290-3294. https://doi.org/10.1002/anie.201511018

Cao YY, Gan ZS, Jia BH, et al., 2011. High-photosensitive resin for super-resolution direct-laser-writing based on photoinhibited polymerization. *Opt Expr*, 19(20):19486-19494. https://doi.org/10.1364/OE.19.019486

Chen XD, Zou CL, Gong ZJ, et al., 2015. Subdiffraction optical manipulation of the charge state of nitrogen vacancy center in diamond. *Light Sci Appl*, 4(1):e230. https://doi.org/10.1038/lsa.2015.3

Chen ZG, Taflove A, Backman V, 2004. Photonic nanojet enhancement of backscattering of light by nanoparticles: a potential novel visible-light ultramicroscopy technique. *Opt Expr*, 12(7):1214-1220. https://doi.org/10.1364/OPEX.12.001214

Chmyrov A, Keller J, Grotjohann T, et al., 2013. Nanoscopy with more than 100,000 'doughnuts'. *Nat Methods*, 10(8):737-740. https://doi.org/10.1038/nmeth.2556

Cordes T, Strackharn M, Stahl SW, et al., 2010. Resolving single-molecule assembled patterns with superresolution blink-microscopy. *Nano Lett*, 10(2):645-651. https://doi.org/10.1021/nl903730r

Cox S, Rosten E, Monypenny J, et al., 2012. Bayesian localization microscopy reveals nanoscale podosome dynamics. *Nat Methods*, 9(2):195-200. https://doi.org/10.1038/nmeth.1812

Darafsheh A, 2013. Optical Super-Resolution and Periodical Focusing Effects by Dielectric Microspheres. PhD Thesis, The University of North Carolina at Charlotte, North Carolina, USA.

Darafsheh A, Walsh GF, Dal Negro L, et al., 2012. Optical super-resolution by high-index liquid-immersed microspheres. *Appl Phys Lett*, 101(14):141128. https://doi.org/10.1063/1.4757600

Darafsheh A, Limberopoulos NI, Derov JS, et al., 2014. Advantages of microsphere-assisted super-resolution imaging technique over solid immersion lens and confocal microscopies. *Appl Phys Lett*, 104(6):061117. https://doi.org/10.1063/1.4864760

Davis HC, Ramesh P, Bhatnagar A, et al., 2018. Mapping the microscale origins of magnetic resonance image contrast with subcellular diamond magnetometry. *Nat Commun*, 9(1):131. https://doi.org/10.1038/s41467-017-02471-7

Degen CL, Poggio M, Mamin HJ, et al., 2009. Nanoscale magnetic resonance imaging. *Proc Nat Acad Sci USA*, 106(5):1313-1317. https://doi.org/10.1073/pnas.0812068106

de Luca GM, Breedijk RMP, Brandt RAJ, et al., 2013. Re-scan confocal microscopy: scanning twice for better resolution. *Biomed Opt Expr*, 4(11):2644-2656. https://doi.org/10.1364/BOE.4.002644

Dertinger T, Colyer R, Iyer G, et al., 2009. Fast, background-free, 3D super-resolution optical fluctuation imaging (SOFI). *Proc Nat Acad Sci USA*, 106(52):22287-22292. https://doi.org/10.1073/pnas.0907866106

Dertinger T, Colyer R, Vogel R, et al., 2012. Superresolution optical fluctuation imaging (SOFI). In: Zahavy E, Ordentlich A, Yitzhaki S, et al. (Eds.), Nano-biotechnology for Biomedical and Diagnostic Research. Springer, Dordrecht, Netherlands, p.17-21. https://doi.org/10.1007/978-94-007-2555-3_2

D'Este E, Kamin D, Göttfert F, et al., 2015. STED nanoscopy reveals the ubiquity of subcortical cytoskeleton periodicity in living neurons. *Cell Rep*, 10(8):1246-1251. https://doi.org/10.1016/j.celrep.2015.02.007

Dickson RM, Cubitt AB, Tsien RY, et al., 1997. On/off blinking and switching behaviour of single molecules of green fluorescent protein. *Nature*, 388(6640):355-358. https://doi.org/10.1038/41048

Donnert G, Keller J, Wurm CA, et al., 2007. Two-color far-field fluorescence nanoscopy. *Biophys J*, 92(8): L67-L69. https://doi.org/10.1529/biophysj.107.104497

Dunin-Borkowski RE, McCartney MR, Frankel RB, et al., 1998. Magnetic microstructure of magnetotactic bacteria by electron holography. *Science*, 282(5395):1868-1870. https://doi.org/10.1126/science.282.5395.1868

Dyba M, Hell SW, 2002. Focal spots of size λ/23 open up far-field florescence microscopy at 33 nm axial resolution. *Phys Rev Lett*, 88(16):163901. https://doi.org/10.1103/PhysRevLett.88.163901

Farahani JN, Schibler MJ, Bentolila LA, 2010. Stimulated emission depletion (STED) microscopy: from theory to practice. *Microsc Sci Technol Appl Educ*, 2(4): 1539-1547.

Ferrand P, Wenger J, Devilez A, et al., 2008. Direct imaging of photonic nanojets. *Opt Expr*, 16(10):6930-6940. https://doi.org/10.1364/OE.16.006930

Finkler A, Segev Y, Myasoedov Y, et al., 2010. Self-aligned nanoscale SQUID on a tip. *Nano Lett*, 10(3):1046-1049. https://doi.org/10.1021/nl100009r

Fiolka R, Shao L, Rego EH, et al., 2012. Time-lapse two-color 3D imaging of live cells with doubled resolution using structured illumination. *Proc Nat Acad Sci USA*, 109(14): 5311-5315. https://doi.org/10.1073/pnas.1119262109

Fischer J, Wegener M, 2011. Three-dimensional direct laser writing inspired by stimulated-emission-depletion microscopy. *Opt Mater Expr*, 1(4):614-624. https://doi.org/10.1364/OME.1.000614

Fischer J, Wegener M, 2013. Three-dimensional optical laser lithography beyond the diffraction limit. *Laser Photon Rev*, 7(1):22-44. https://doi.org/10.1002/lpor.201100046

Fischer J, von Freymann G, Wegener M, 2010. The materials challenge in diffraction-unlimited direct-laser-writing optical lithography. *Adv Mater*, 22(32):3578-3582. https://doi.org/10.1002/adma.201000892

Fölling J, Bossi M, Bock H, et al., 2008. Fluorescence nanoscopy by ground-state depletion and single-molecule return. *Nat Methods*, 5(11):943-945. https://doi.org/10.1038/NMETH.1257

Galiani S, Waithe D, Reglinski K, et al., 2016. Super-resolution microscopy reveals compartmentalization of peroxisomal membrane proteins. *J Biol Chem*, 291(33): 16948-16962. https://doi.org/10.1074/jbc.M116.734038

Gan ZS, Cao YY, Evans RA, et al., 2013. Three-dimensional deep sub-diffraction optical beam lithography with 9 nm feature size. *Nat Commun*, 4:2061. https://doi.org/10.1038/ncomms3061

Geissbuehler S, Sharipov A, Godinat A, et al., 2014. Live-cell multiplane three-dimensional super-resolution optical fluctuation imaging. *Nat Commun*, 5:5830. https://doi.org/10.1038/ncomms6830

Glenn DR, Lee K, Park H, et al., 2015. Single-cell magnetic imaging using a quantum diamond microscope. *Nat Methods*, 12(8):736-738. https://doi.org/10.1038/nmeth.3449

Göttfert F, Wurm CA, Mueller V, et al., 2013. Coaligned dual-channel STED nanoscopy and molecular diffusion analysis at 20 nm resolution. *Biophys J*, 105(1): L01-L03. https://doi.org/10.1016/j.bpj.2013.05.029

Gregor I, Spiecker M, Petrovsky R, et al., 2017. Rapid nonlinear image scanning microscopy. *Nat Methods*, 14(11):1087-1089. https://doi.org/10.1038/nmeth.4467

Grotjohann T, Testa I, Leutenegger M, et al., 2011. Diffraction-unlimited all-optical imaging and writing with a photochromic GFP. *Nature*, 478(7368):204-208. https://doi.org/10.1038/nature10497

Gruber A, Dräbenstedt A, Tietz C, et al., 1997. Scanning confocal optical microscopy and magnetic resonance on single defect centers. *Science*, 276(5321):2012-2014. https://doi.org/10.1126/science.276.5321.2012

Gu M, 1996. Principles of Three-Dimensional Imaging in Confocal Microscopes. World Scientific, Singapore.

Gu M, 2000. Advanced Optical Imaging Theory. Springer, Berlin, Germany.

Gu M, Cao YY, Castelletto S, et al., 2013. Super-resolving single nitrogen vacancy centers within single nanodiamonds using a localization microscope. *Opt Expr*, 21(15):17639-17646. https://doi.org/10.1364/OE.21.017639

Gu M, Kang H, Li XP, 2014. Breaking the diffraction-limited resolution barrier in fiber-optical two-photon fluorescence endoscopy by an azimuthally-polarized beam. *Sci Rep*, 4:3627. https://doi.org/10.1038/srep03627

Gu M, Zhang QM, Lamon S, 2016. Nanomaterials for optical data storage. *Nat Rev Mater*, 1(12):16070. https://doi.org/10.1038/natrevmats.2016.70

Gustafsson MGL, 2000. Surpassing the lateral resolution limit by a factor of two using structured illumination microscopy. *J Microsc*, 198(2):82-87. https://doi.org/10.1046/j.1365-2818.2000.00710.x

Gustafsson MGL, 2005. Nonlinear structured-illumination microscopy: wide-field fluorescence imaging with theoretically unlimited resolution. *Proc Nat Acad Sci USA*, 102(37):13081-13086. https://doi.org/10.1073/pnas.0406877102

Gustafsson MGL, Shao L, Carlton PM, et al., 2008. Three-dimensional resolution doubling in wide-field fluorescence microscopy by structured illumination. *Biophys J*, 94(12):4957-4970. https://doi.org/10.1529/biophysj.107.120345

Han S, Xiong Y, Genov D, et al., 2008. Ray optics at a deep-subwavelength scale: a transformation optics approach. *Nano Lett*, 8(12):4243-4247.

https://doi.org/10.1021/nl801942x

Hell SW, 2007. Far-field optical nanoscopy. *Science*, 316(5828):1153-1158. https://doi.org/10.1126/science.1137395

Hell SW, Kroug M, 1995. Ground-state-depletion fluorscence microscopy: a concept for breaking the diffraction resolution limit. *Appl Phys B*, 60(5):495-497. https://doi.org/10.1007/BF01081333

Hell SW, Wichmann J, 1994. Breaking the diffraction resolution limit by stimulated emission: stimulated-emission-depletion fluorescence microscopy. *Opt Lett*, 19(11):780-782. https://doi.org/10.1364/OL.19.000780

Hess ST, Girirajan TPK, Mason MD, 2006. Ultra-high resolution imaging by fluorescence photoactivation localization microscopy. *Biophys J*, 91(11):4258-4272. https://doi.org/10.1529/biophysj.106.091116

Hirvonen LM, Wicker K, Mandula O, et al., 2009. Structured illumination microscopy of a living cell. *Eur Biophys J*, 38(6):807-812. https://doi.org/10.1007/s00249-009-0501-6

Hofmann M, Eggeling C, Jakobs S, et al., 2005. Breaking the diffraction barrier in fluorescence microscopy at low light intensities by using reversibly photoswitchable proteins. *Proc Nat Acad Sci USA*, 102(49):17565-17569. https://doi.org/10.1073/pnas.0506010102

Hortigon-Vinagre MP, Zamora V, Burton FL, et al., 2016. The use of ratiometric fluorescence measurements of the voltage sensitive dye Di-4-ANEPPS to examine action potential characteristics and drug effects on human induced pluripotent stem cell-derived cardiomyocytes. *Toxicol Sci*, 154(2):320-331. https://doi.org/10.1093/toxsci/kfw171

Hu YS, Nan XL, Sengupta P, et al., 2013. Accelerating 3B single-molecule super-resolution microscopy with cloud computing. *Nat Methods*, 10(2):96-97. https://doi.org/10.1038/nmeth.2335

Huang B, Jones SA, Brandenburg B, et al., 2008a. Whole-cell 3D STORM reveals interactions between cellular structures with nanometer-scale resolution. *Nat Methods*, 5(12):1047-1052. https://doi.org/10.1038/nmeth.1274

Huang B, Wang WQ, Bates M, et al., 2008b. Three-dimensional super-resolution imaging by stochastic optical reconstruction microscopy. *Science*, 319(5864): 810-813. https://doi.org/10.1126/science.1153529

Ikonen P, Simovski C, Tretyakov S, et al., 2007. Magnification of subwavelength field distributions at microwave frequencies using a wire medium slab operating in the canalization regime. *Appl Phys Lett*, 91(10):104102. https://doi.org/10.1063/1.2767996

Jacob Z, Alekseyev LV, Narimanov E, 2006. *Optical hyperlens*: far-field imaging beyond the diffraction limit. *Opt Expr*, 14(18):8247-8256. https://doi.org/10.1364/OE.14.008247

Jaskula JC, Bauch E, Arroyo-Camejo S, et al., 2017. Superresolution optical magnetic imaging and spectroscopy using individual electronic spins in diamond. *Opt Expr*, 25(10):11048-11064. https://doi.org/10.1364/OE.25.011048

Jones SA, Shim SH, He J, et al., 2011. Fast, three-dimensional super-resolution imaging of live cells. *Nat Methods*, 8(6):499-505. https://doi.org/10.1038/nmeth.1605

Juette MF, Gould TJ, Lessard MD, et al., 2008. Three-dimensional sub-100 nm resolution fluorescence microscopy of thick samples. *Nat Methods*, 5(6):527-529. https://doi.org/10.1038/nmeth.1211

Kildishev AV, Shalaev VM, 2008. Engineering space for light via transformation optics. *Opt Lett*, 33(1):43-45. https://doi.org/10.1364/OL.33.000043

Kim MS, Scharf T, Haq MT, et al., 2011. Subwavelength-size solid immersion lens. *Opt Lett*, 36(19):3930-3932. https://doi.org/10.1364/OL.36.003930

Klar TA, Hell SW, 1999. Subdiffraction resolution in far-field fluorescence microscopy. *Opt Lett*, 24(14):954-956. https://doi.org/10.1364/OL.24.000954

Kner P, Chhun BB, Griffis ER, et al., 2009. Super-resolution video microscopy of live cells by structured illumination. *Nat Methods*, 6(5):339-342. https://doi.org/10.1038/nmeth.1324

Kwon J, Hwang J, Park J, et al., 2015. RESOLFT nanoscopy with photoswitchable organic fluorophores. *Sci Rep*, 5:17804. https://doi.org/10.1038/srep17804

Lakadamyali M, Babcock H, Bates M, et al., 2012. 3D multicolor super-resolution imaging offers improved accuracy in neuron tracing. *PLoS One*, 7(1):e30826. https://doi.org/10.1371/journal.pone.0030826

Lee JY, Hong BH, Kim WY, et al., 2009. Near-field focusing and magnification through self-assembled nanoscale spherical lenses. *Nature*, 460(7254):498-501. https://doi.org/10.1038/nature08173

Lee SC, Kim K, Kim J, et al., 2009. MR microscopy of micron scale structures. *Magn Reson Imag*, 27(6):828-833. https://doi.org/10.1016/j.mri.2009.01.002

Le Sage D, Arai K, Glenn DR, et al., 2013. Optical magnetic imaging of living cells. *Nature*, 496(7446):486-489. https://doi.org/10.1038/nature12072

Lesterlin C, Ball G, Schermelleh L, et al., 2014. RecA bundles mediate homology pairing between distant sisters during DNA break repair. *Nature*, 506(7487):249-253. https://doi.org/10.1038/nature12868

Li D, Shao L, Chen BC, et al., 2015. Extended-resolution structured illumination imaging of endocytic and cytoskeletal dynamics. *Science*, 349(6251):3500. https://doi.org/10.1126/science.aab3500

Li L, Guo W, Yan YZ, et al., 2013. Label-free super-resolution imaging of adenoviruses by submerged microsphere optical nanoscopy. *Light Sci Appl*, 2(9):e104. https://doi.org/10.1038/lsa.2013.60

Li LJ, Gattass RR, Gershgoren E, et al., 2009. Achieving $\lambda/20$ resolution by one-color initiation and deactivation of polymerization. *Science*, 324(5929):910-913. https://doi.org/10.1126/science.1168996

Lidke KA, Rieger B, Jovin TM, et al., 2005. Superresolution

by localization of quantum dots using blinking statistics. *Opt Expr*, 13(18):7052-7062. https://doi.org/10.1364/OPEX.13.007052

Liu ZW, Lee H, Xiong Y, et al., 2007. Far-field optical hyperlens magnifying sub-diffraction-limited objects. *Science*, 315(5819):1686. https://doi.org/10.1126/science.1137368

Lukinavičius G, Reymond L, Umezawa K, et al., 2016. Fluorogenic probes for multicolor imaging in living cells. *J Am Chem Soc*, 138(30):9365-9368. https://doi.org/10.1021/jacs.6b04782

Ma CB, Liu ZW, 2010a. Focusing light into deep subwavelength using metamaterial immersion lenses. *Opt Expr*, 18(5):4838-4844. https://doi.org/10.1364/OE.18.004838

Ma CB, Liu ZW, 2010b. A super resolution metalens with phase compensation mechanism. *Appl Phys Lett*, 96(18): 183103. https://doi.org/10.1063/1.3427199

Ma CB, Liu ZW, 2011. Designing super-resolution metalenses by the combination of metamaterials and nanoscale plasmonic waveguide couplers. *J Nanophoton*, 5(1): 051604. https://doi.org/10.1117/1.3579159

Ma CB, Escobar MA, Liu ZW, 2011. Extraordinary light focusing and Fourier transform properties of gradient-index metalenses. *Phys Rev B*, 84(19):195142. https://doi.org/10.1103/PhysRevB.84.195142

Mason DR, Jouravlev MV, Kim KS, 2010. Enhanced resolution beyond the Abbe diffraction limit with wavelength-scale solid immersion lenses. *Opt Lett*, 35(12):2007-2009. https://doi.org/10.1364/OL.35.002007

Moerner WE, Kador L, 1989. Optical detection and spectroscopy of single molecules in a solid. *Phys Rev Lett*, 62(21):2535-2538. https://doi.org/10.1103/PhysRevLett.62.2535

Müller CB, Enderlein J, 2010. Image scanning microscopy. *Phys Rev Lett*, 104(19):198101. https://doi.org/10.1103/PhysRevLett.104.198101

Nahidiazar L, Agronskaia AV, Broertjes J, et al., 2016. Optimizing imaging conditions for demanding multi-color super resolution localization microscopy. *PLoS One*, 11(7):e0158884. https://doi.org/10.1371/journal.pone.0158884

Ono A, Kato JI, Kawata S, 2005. Subwavelength optical imaging through a metallic nanorod array. *Phys Rev Lett*, 95(26):267407. https://doi.org/10.1103/PhysRevLett.95.267407

Pan L, Park Y, Xiong Y, et al., 2011. Maskless plasmonic lithography at 22 nm resolution. *Sci Rep*, 1:175. https://doi.org/10.1038/srep00175

Parazzoli CG, Greegor RB, Nielsen JA, et al., 2004. Performance of a negative index of refraction lens. *Appl Phys Lett*, 84(17):3232-3234. https://doi.org/10.1063/1.1728304

Patterson G, Davidson M, Manley S, 2010. Superresolution imaging using single-molecule localization. *Ann Rev Phys Chem*, 61:345-367 https://doi.org/10.1146/annurev.physchem.012809.103444

Pendry JB, Ramakrishna SA, 2002. Near-field lenses in two dimensions. *J Phys Condens Matter*, 14(36):8463-8479. https://doi.org/10.1088/0953-8984/14/36/306

Pham LM, Le Sage D, Stanwix PL, et al., 2011. Magnetic field imaging with nitrogen-vacancy ensembles. *New J Phys*, 13:045021. https://doi.org/10.1088/1367-2630/13/4/045021

Podolskiy VA, Alekseyev LV, Narimanov EE, 2005. Strongly anisotropic media: the THz perspectives of left-handed materials. *J Mod Opt*, 52(16):2343-2349. https://doi.org/10.1080/09500340500275579

Qin SY, Yin H, Yang CL, et al., 2016. A magnetic protein biocompass. *Nat Mater*, 15(2):217-226. https://doi.org/10.1038/nmat4484

Rai-Choudhury P, 1997. Handbook of Microlithography, Micromachining, and Microfabrication. Vol. 1. Institution of Engineering and Technology, London, UK.

Rankin BR, Moneron G, Wurm CA, et al., 2011. Nanoscopy in a living multicellular organism expressing GFP. *Biophys J*, 100(12):L63-L65. https://doi.org/10.1016/j.bpj.2011.05.020

Rego EH, Shao L, Macklin JJ, et al., 2012. Nonlinear structured-illumination microscopy with a photo-switchable protein reveals cellular structures at 50-nm resolution. *Proc Nat Acad Sci USA*, 109(3): E135-E143. https://doi.org/10.1073/pnas.1107547108

Rho J, Ye ZL, Xiong Y, et al., 2010. Spherical hyperlens for two-dimensional sub-diffractional imaging at visible frequencies. *Nat Commun*, 1:143. https://doi.org/10.1038/ncomms1148

Rittweger E, Han KY, Irvine SE, et al., 2009a. STED microscopy reveals crystal colour centres with nanometric resolution. *Nat Photon*, 3(3):144-147. https://doi.org/10.1038/nphoton.2009.2

Rittweger E, Wildanger D, Hell SW, 2009b. Far-field fluorescence nanoscopy of diamond color centers by ground state depletion. *Europhys Lett*, 86(1):14001. https://doi.org/10.1209/0295-5075/86/14001

Roth S, Sheppard CJR, Wicker K, et al., 2013. Optical photon reassignment microscopy (OPRA). *Opt Nanosc*, 2:5. https://doi.org/10.1186/2192-2853-2-5

Rust MJ, Bates M, Zhuang XW, 2006. Sub-diffraction-limit imaging by stochastic optical reconstruction microscopy (STORM). *Nat Methods*, 3(10):793-796. https://doi.org/10.1038/nmeth929

Sanamrad A, Persson F, Lundius EG, et al., 2014. Single-particle tracking reveals that free ribosomal subunits are not excluded from the *Escherichia coli* nucleoid. *Proc Nat Acad Sci USA*, 111(31):11413-11418. https://doi.org/10.1073/pnas.1411558111

Schermelleh L, Carlton PM, Haase S, et al., 2008. Subdiffraction multicolor imaging of the nuclear periphery with 3D structured illumination microscopy. *Science*, 320(5881):1332-1336.

https://doi.org/10.1126/science.1156947

Schmidt R, Wurm CA, Jakobs S, et al., 2008. Spherical nanosized focal spot unravels the interior of cells. *Nat Methods*, 5(6):539-544. https://doi.org/10.1038/nmeth.1214

Schulz O, Pieper C, Clever M, et al., 2013. Resolution doubling in fluorescence microscopy with confocal spinning-disk image scanning microscopy. *Proc Nat Acad Sci USA*, 110(52):21000-21005. https://doi.org/10.1073/pnas.1315858110

Scott TF, Kowalski BA, Sullivan AC, et al., 2009. Two-color single-photon photoinitiation and photoinhibition for subdiffraction photolithography. *Science*, 324(5929):913-917. https://doi.org/10.1126/science.1167610

Sednev MV, Belov VN, Hell SW, 2015. Fluorescent dyes with large Stokes shifts for super-resolution optical microscopy of biological objects: a review. *Methods Appl Fluoresc*, 3(4):042004. https://doi.org/10.1088/2050-6120/3/4/042004

Shao L, Kner P, Rego EH, et al., 2011. Super-resolution 3D microscopy of live whole cells using structured illumination. *Nat Methods*, 8(12):1044-1046. https://doi.org/10.1038/nmeth.1734

Sheppard CJR, 1988. Super-resolution in confocal imaging. *Optik*, 80(2):53-54.

Sheppard CJR, Mehta SB, Heintzmann R, 2013. Superresolution by image scanning microscopy using pixel reassignment. *Opt Lett*, 38(15):2889-2892. https://doi.org/10.1364/OL.38.002889

Shroff H, Galbraith CG, Galbraith JA, et al., 2008. Live-cell photoactivated localization microscopy of nanoscale adhesion dynamics. *Nat Methods*, 5(5):417-423. https://doi.org/10.1038/nmeth.1202

Shtengel G, Galbraith JA, Galbraith CG, et al., 2009. Interferometric fluorescent super-resolution microscopy resolves 3D cellular ultrastructure. *Proc Nat Acad Sci USA*, 106(9):3125-3130. https://doi.org/10.1073/pnas.0813131106

Shvets G, Trendafilov S, Pendry JB, et al., 2007. Guiding, focusing, and sensing on the subwavelength scale using metallic wire arrays. *Phys Rev Lett*, 99(5):053903. https://doi.org/10.1103/PhysRevLett.99.053903

Sidenstein SC, D'Este E, Böhm MJ, et al., 2016. Multicolour multilevel STED nanoscopy of actin/spectrin organization at synapses. *Sci Rep*, 6:26725. https://doi.org/10.1038/srep26725

Subach FV, Patterson GH, Manley S, et al., 2009. Photoactivatable mCherry for high-resolution two-color fluorescence microscopy. *Nat Methods*, 6(2):153-159. https://doi.org/10.1038/nmeth.1298

Sun ZJ, Kim HK, 2004. Refractive transmission of light and beam shaping with metallic nano-optic lenses. *Appl Phys Lett*, 85(4):642. https://doi.org/10.1063/1.1776327

Testa I, Wurm CA, Medda R, et al., 2010. Multicolor fluorescence nanoscopy in fixed and living cells by exciting conventional fluorophores with a single wavelength. *Biophys J*, 99(8):2686-2694. https://doi.org/10.1016/j.bpj.2010.08.012

Tønnesen J, Nadrigny F, Willig KI, et al., 2011. Two-color STED microscopy of living synapses using a single laser-beam pair. *Biophys J*, 101(10):2545-2552. https://doi.org/10.1016/j.bpj.2011.10.011

Tsang M, Psaltis D, 2008. Magnifying perfect lens and superlens design by coordinate transformation. *Phys Rev B*, 77(3):035122. https://doi.org/10.1103/PhysRevB.77.035122

Uno SN, Kamiya M, Yoshihara T, et al., 2014. A spontaneously blinking fluorophore based on intramolecular spirocyclization for live-cell super-resolution imaging. *Nat Chem*, 6(8):681-689. https://doi.org/10.1038/nchem.2002

Verslegers L, Catrysse PB, Yu ZF, et al., 2009a. Deep-subwavelength focusing and steering of light in an aperiodic metallic waveguide array. *Phys Rev Lett*, 103(3):033902. https://doi.org/10.1103/PhysRevLett.103.033902

Verslegers L, Catrysse PB, Yu ZF, et al., 2009b. Planar lenses based on nanoscale slit arrays in a metallic film. *Nano Lett*, 9(1):235-238. https://doi.org/10.1021/nl802830y

Vogelsang J, Kasper R, Steinhauer C, et al., 2008. A reducing and oxidizing system minimizes photobleaching and blinking of fluorescent dyes. *Angew Chem Int Ed*, 47(29):5465-5469. https://doi.org/10.1002/anie.200801518

Wang ZB, Guo W, Li L, et al., 2011. Optical virtual imaging at 50 nm lateral resolution with a white-light nanoscope. *Nat Commun*, 2:218. https://doi.org/10.1038/ncomms1211

Westphal V, Hell SW, 2005. Nanoscale resolution in the focal plane of an optical microscope. *Phys Rev Lett*, 94(14): 143903. https://doi.org/10.1103/PhysRevLett.94.143903

Westphal V, Rizzoli SO, Lauterbach MA, et al., 2008. Video-rate far-field optical nanoscopy dissects synaptic vesicle movement. *Science*, 320(5873):246-249. https://doi.org/10.1126/science.1154228

Wiedenmann J, Ivanchenko S, Oswald F, et al., 2004. EosFP, a fluorescent marker protein with UV-inducible green-to-red fluorescence conversion. *Proc Nat Acad Sci USA*, 101(45):15905-15910. https://doi.org/10.1073/pnas.0403668101

Willig KI, Harke B, Medda R, et al., 2007. STED microscopy with continuous wave beams. *Nat Methods*, 4(11):915-918. https://doi.org/10.1038/nmeth1108

Winter FR, Loidolt M, Westphal V, et al., 2017. Multicolour nanoscopy of fixed and living cells with a single STED beam and hyperspectral detection. *Sci Rep*, 7:46492. https://doi.org/10.1038/srep46492

Xiong Y, Liu ZW, Zhang X, 2009. A simple design of flat hyperlens for lithography and imaging with half-pitch resolution down to 20 nm. *Appl Phys Lett*, 94(20): 203108. https://doi.org/10.1063/1.3141457

Xu K, Zhong GS, Zhuang XW, 2013. Actin, spectrin, and associated proteins form a periodic cytoskeletal structure

in axons. *Science*, 339(6118):452-456. https://doi.org/10.1126/science.1232251

Yang H, Moullan N, Auwerx J, et al., 2014. Super-resolution biological microscopy using virtual imaging by a microsphere nanoscope. *Small*, 10(9):1712-1718. https://doi.org/10.1002/smll.201302942

Yang H, Trouillon R, Huszka G, et al., 2016. Super-resolution imaging of a dielectric microsphere is governed by the waist of its photonic nanojet. *Nano Lett*, 16(8):4862-4870. https://doi.org/10.1021/acs.nanolett.6b01255

Yao J, Liu ZW, Liu YM, et al., 2008. Optical negative refraction in bulk metamaterials of nanowires. *Science*, 321(5891):930. https://doi.org/10.1126/science.1157566

York AG, Parekh SH, Nogare DD, et al., 2012. Resolution doubling in live, multicellular organisms via multifocal structured illumination microscopy. *Nat Methods*, 9(7):749-754. https://doi.org/10.1038/nmeth.2025

York AG, Chandris P, Nogare DD, et al., 2013. Instant super-resolution imaging in live cells and embryos via analog image processing. *Nat Methods*, 10(11):1122-1126. https://doi.org/10.1038/nmeth.2687

Zhang X, Liu ZW, 2008. Superlenses to overcome the diffraction limit. *Nat Mater*, 7(6):435-441. https://doi.org/10.1038/nmat2141

Zhao Y, Palikaras G, Belov PA, et al., 2010. Magnification of subwavelength field distributions using a tapered array of metallic wires with planar interfaces and an embedded dielectric phase compensator. *New J Phys*, 12(10):103045. https://doi.org/10.1088/1367-2630/12/10/103045